Supplementary information

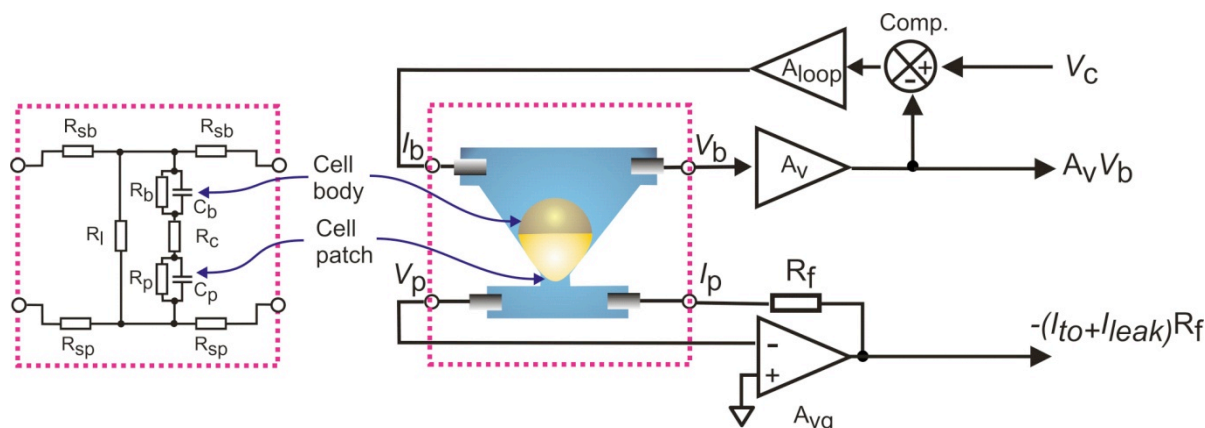### Description of the ATOVC

Fig. S1 Simplified schematic of the ATOVC (not drawn to scale) as used for the experiments described, in which the body membrane exposed to the upper compartment fluid is permeabilized to gain electrical access to the cytosol and thereby allow voltage clamping of the patch exposed to the lower compartment (microfluidic channel). Two electrodes make contact with solution in the upper compartment (I_b, V_b) and lower compartment (I_p, V_p) respectively. The equivalent circuit of the boxed region, representing the oocyte positioned in the core module, is also depicted. This is an AC equivalent model used in simulations (see below) and omits the membrane potential. R_{sb} and R_{sp} represent the equivalent resistances of the electrodes and fluid access to the body (upper) and patch (lower) membranes, R_l is the leak resistance, R_b and C_b are the lumped resistance and capacitance of the cell body, Rc is the lumped cytosolic resistance and R_P and C_P are the membrane patch resistance and capacitance, respectively. The voltage clamp electronics comprises two components that connect to the lower and upper compartments, respectively: (i) a virtual ground amplifier (A_{vg}) defines the potential in the lower compartment (approximating the potential at the external surface of the patch) to 0 V and acts as a transimpedance stage that outputs a voltage proportional to the total current (leak (I_{leak}) and transoocyte (I_{to})); (ii) a feedback amplifier arrangement, comprising amplifier A_v, a comparator and loop gain amplifier (A_{loop}) senses the electrical potential in the upper compartment and compares a scaled version of this (A_v V_b) to the external command voltage input (V_c). The feedback amplifier (A_{loop}) drives current ($I_{leak} + I_{to}$) to maintain the transoocyte potential at the desired value.

The arrangement shown in Fig S1 permits voltage clamping of the patch membrane by controlling the cytosolic potential and assumes adequate electrical access to the cytosol from the upper compartment has been established. The same arrangement could be used for transimpedance measurements. Furthermore, by rearranging the connections to the core module so that the potential in the lower compartment is externally defined, and the upper compartment is held at 0 V, a loose macropatch configuration would be created.

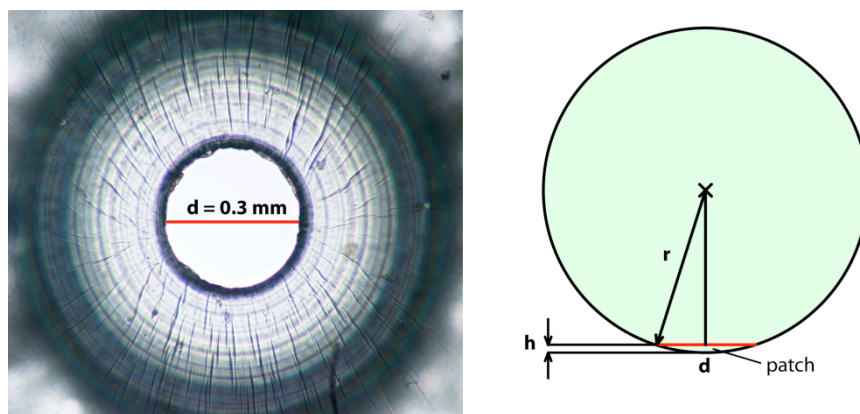### Patch surface area considerations

Fig. S2 Left: Micrograph showing the oocyte immobilization site from above. The patch hole diameter is 0.3 mm. Right: Idealised cross-section of the oocyte showing geometrical parameters.

The patch opening diameter was chosen on the basis of maintaining cell stability, considerations of the electrical properties of the cell and having rapid superfusion of the exposed area. Too large an opening would result in poor electrical access to the cytosol whereas too small an opening would compromise the signal-to-noise ratio for the patch current.
The surface area (S) of a sphere with radius r is given by: $S = 4 \pi r^2$.
The patch area (curved surface area of the cap) is calculated using the following equations: $S_P = 2 \pi r h$ with $h = r - \sqrt{(r^2 - a^2)}$.
where, h is the height of the patch and a the patch radius. For a sphere with r=0.5 mm (typical for *Xenopus laevis* oocytes) and a =0.15 mm (Fig. S2) the surface area ratio is:
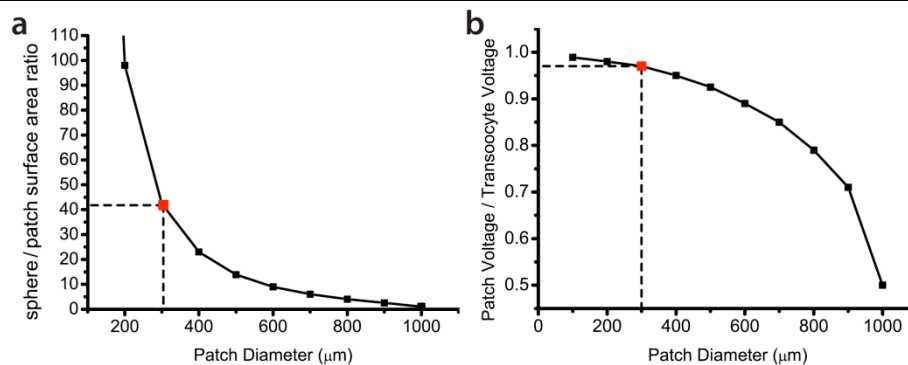
$$\frac{S}{S_P} \approx 43$$

Fig. S3 The dependence of the surface ratio (a) and voltage ratio (b) plotted as function of the patch hole diameter. The values were obtained by simulation (Fig. S4) for a typical oocyte diameter of 1 mm and an AC clamp voltage at 10 Hz. Actual values chosen for our design are indicated (dashed lines/red symbols).

The relationship between the impedance ratio of the two membrane parts and their respective surface areas can be expressed using the following equation:

$$\frac{R_B}{R_P} = \frac{C_P}{C_B} = \frac{4\pi r^2}{S_P} - 1$$

where r: radius of the oocyte and S_P: patch area. Here we take the apparent geometrical areas and ignore the increased surface area of the oocyte due to the microvilli and invaginations. This would simply scale the calculated areas equally.

Assuming homogeneous distribution of membrane conductance the membrane impedances of the two regions will differ, according to the ratio of the membrane areas of each region. Consequently, changes in the transoocyte current will mainly result from changes in the impedance of the patch membrane due to its much higher impedance compared to the impedance of the body membrane.

Thus, even though the oocyte is effectively voltage clamped across two membranes, the largest fraction of applied AC voltage falls across the patched membrane, i.e. by having a large ratio between the non-patched area and the patched area, a voltage clamp from the cytosol across a single membrane is approximated (Fig. S3b). In practice, the measured values will deviate somewhat from the calculated values due to the deformation of the immobilized oocyte. Nevertheless, this relation is useful for comparing membrane currents of the ATOVC with membrane currents measured with a conventional instrument (TEVC). Moreover, to simplify the analysis, this model ignores the effect of inhomogeneities of membrane access resistance close to the patch hole.
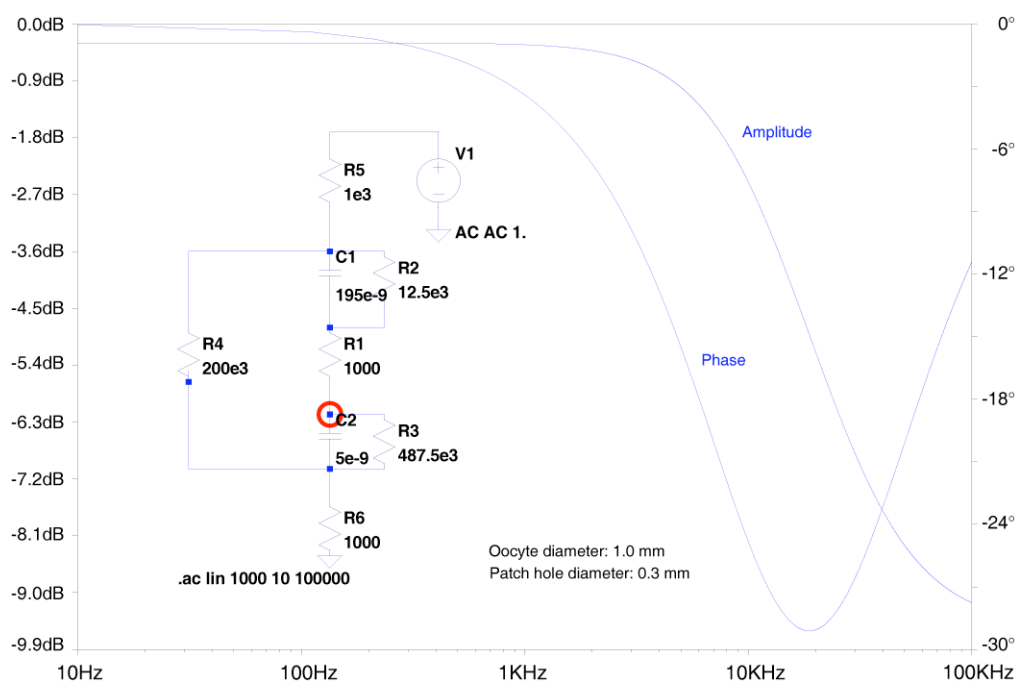
AC impedance analysis of the ATOVC

Fig. S4 Bode plot of the equivalent circuit of the ATOVC (made using LT SPICE IV (Linear Technologies)). The absolute values for the resistances and capacitances are rough estimates. The DC resistance of the entire circuit is typically around 150 kΩ.

A SPICE AC analysis using estimated values for the ATOVC reveals that the patch impedance is reasonably constant up to frequencies around 1 kHz (Fig. S4).
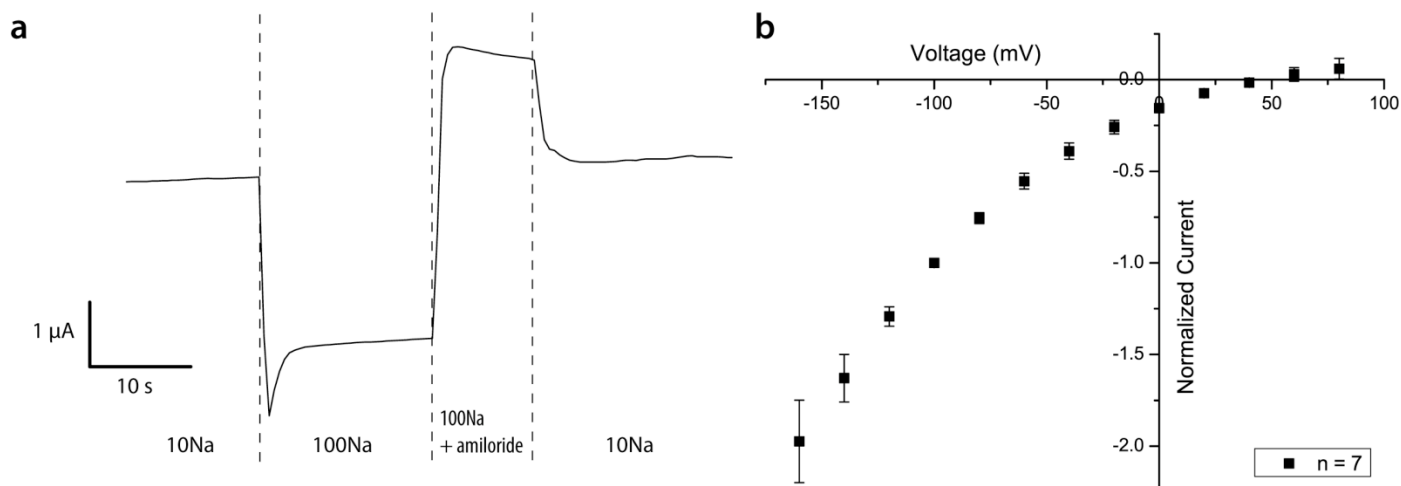
TEVC reference measurements

Fig. S5 (a) Real-time TEVC recording of membrane current from a representative oocyte expressing ENaC and voltage clamped to -50 mV. (b) I-V data from ENaC expressing oocytes (n = 7). Amiloride-sensitive currents were normalized to the current at -100 mV and data pooled (mean ± sem).

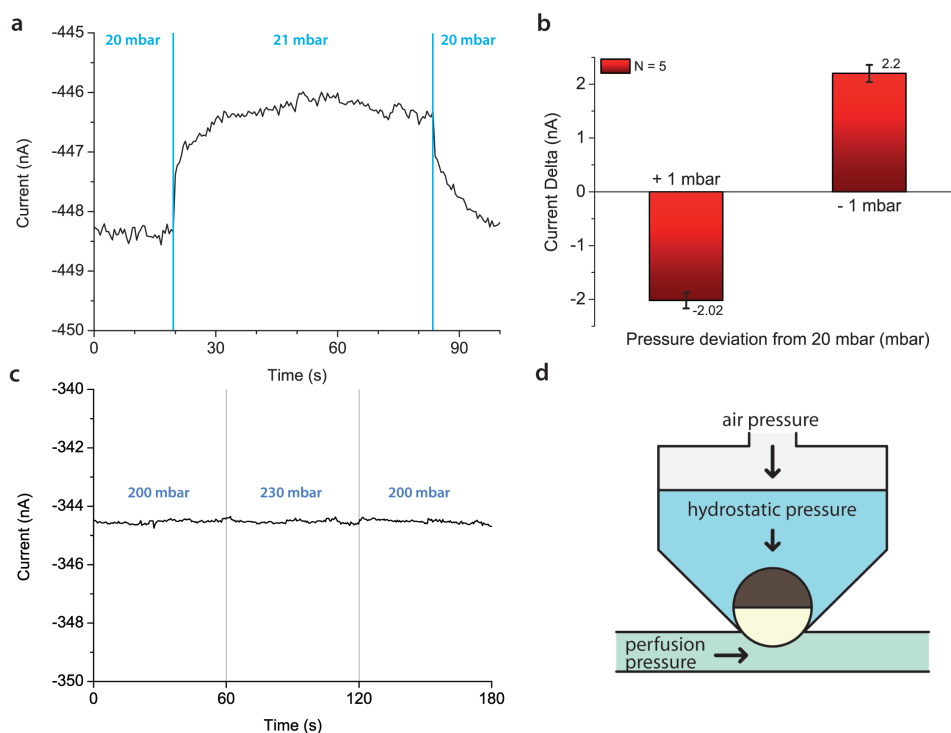**Influence of pressure variations on the leak conductance**

Fig. S6 (a) Time-dependent measurement of leak current varying the air pressure acting on the native oocyte. The transoocyte voltage and the perfusion flow rate were kept constant at -50 mV and 2 μl/s (200 mbar), respectively. (b) Statistical evaluation of 5 oocytes subjected to air pressure variation of 1 mbar in both directions (base pressure 20 mbar). (c) Time-dependent measurement of the leak current varying the perfusion pressure in the microchannel. (d) Scheme showing the direction of the forces (arrows) involved in the experiment.

To study the influence of air pressure variations on the leak conductance a series of experiments were conducted where either the air pressure (Fig. S6a) or the perfusion pressure (Fig. S6c) was varied. These tests demonstrate the system's susceptibility to variations in the immobilization pressure (top pressure) and tolerance to the hydrodynamic resistance of the individual solution pathways. All tests were conducted on native oocytes which have negligible membrane conductance compared to the leak. Therefore, the current resulting from an applied transoocyte voltage is predominantly leak current.

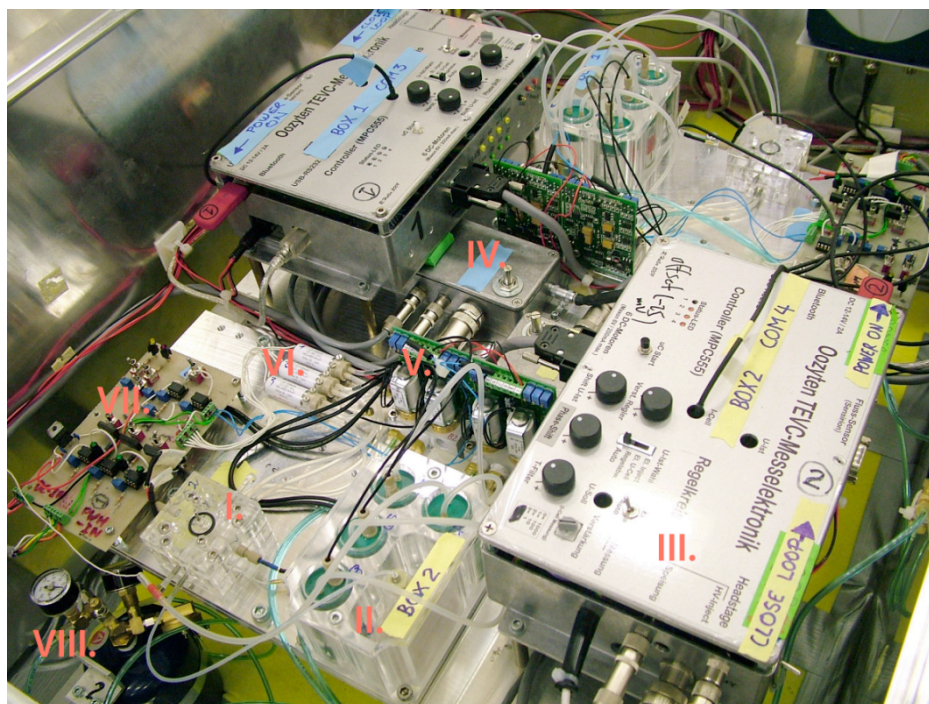**Photograph of the ATOVC setup for parabolic flights**

Fig. S7 Photograph of two identical ATOVC setups. I. ATOVC core module (air pressure tubing not connected). II. Holder for the three solution vials, compensation volume and expandable waste reservoir. III. Voltage clamp hardware and system controller. IV. Preamplifier headstage. V. Electronic pressure regulators. VI. Solenoid valves for solution switching. VII. Control module for manual valve switching. VIII. Air supply bottle.